



Research on the Microscopic Migration Law of CO₂ in Salt Water Storage Based on Pressure Driving

Jing Li and Chuan-zhi Cui^(✉)

College of Petroleum Engineering, China University of Petroleum (East China),
Qingdao, China

ccz2008@126.com

Abstract. CO₂ capture, utilization, and storage (CCUS) is a beneficial measure for controlling carbon emissions and reducing greenhouse gases. At present, most of the studies on CO₂ storage describe the mechanism, calculation of storage volume, calculation of cap breakthrough pressure and CO₂ migration law at the macroscopic level, but there are few studies on the CO₂ transport law in the storage process at the microscopic pore scale. This paper establishes numerical formulas for CO₂ migration and interface characterization at the pore scale based on numerical simulation methods. Using a two-dimensional model of porous media, a pressure-driven approach is used to simulate the microscopic migration characteristics of CO₂ during the storage process of salt water layers. The CO₂ migration law is explained, and the influence of pressure and wettability on the migration law is analyzed. Research has shown that during the injection process, CO₂ will migrate along the mainstream toward the outlet. Meanwhile, due to the density difference between the two phases, CO₂ will migrate upward until it reaches the top of the model. At the end of injection, residual water is mainly distributed at the edges and corners of the model. During the suction process, residual CO₂ gas will be trapped at the top and upper right corner of the model under hydraulic and boundary effects. The increase in injection pressure will reduce the full displacement time and increase the residual gas burial rate. The weakening of wall hydrophilicity will shorten the displacement process time, increase the suction

Copyright 2023, IFEDC Organizing Committee.

This paper was prepared for presentation at the 2023 International Field Exploration and Development Conference in Wuhan, China, 20–22 September 2023.

This paper was selected for presentation by the IFEDC Committee following review of information contained in an abstract submitted by the author(s). Contents of the paper, as presented, have not been reviewed by the IFEDC Technical Team and are subject to correction by the author(s). The material does not necessarily reflect any position of the IFEDC Technical Committee its members. Papers presented at the Conference are subject to publication review by Professional Team of IFEDC Technical Committee. Electronic reproduction, distribution, or storage of any part of this paper for commercial purposes without the written consent of IFEDC Organizing Committee is prohibited. Permission to reproduce in print is restricted to an abstract of not more than 300 words; illustrations may not be copied. The abstract must contain conspicuous acknowledgment of IFEDC. Contact email: paper@ifedc.org.

© The Author(s), under exclusive license to Springer Nature Singapore Pte Ltd. 2024
J. Lin (Ed.): IFEDC 2023, SSGG, pp. 548–557, 2024.
https://doi.org/10.1007/978-981-97-0268-8_42

process time, and gradually reduce the maximum burial rate. This study characterizes the flow pattern of two phases during CO₂ storage in the salt water layer from a microscopic perspective, which has reference significance for further understanding the CO₂ storage mechanism in mines.

Keywords: Pressure driven · Salt water layer · CO₂ storage · Microscopic migration laws · Numerical simulation · Wettability

1 Introduction

With the acceleration of industrialization, the world is facing challenges in addressing climate change and high greenhouse gas emissions. The signing of the Paris Agreement on December 12, 2015, meant that the signatories reached a consensus to cut greenhouse gas emissions and achieve a temperature rise of no more than 2 °C [1]. Current measures to effectively reduce CO₂ emissions include improving resource efficiency; using low-carbon or carbon-free energy; and adopting CO₂ capture, utilization and storage (CCUS) technologies. CO₂ capture, utilization, and storage (CCUS) is the process of capturing industrial emissions of CO₂ for water, oil, gas, and mining applications while achieving carbon sequestration. CCUS technology is still considered the main way to reduce carbon emissions [2–4]. CO₂ storage is mainly achieved by injecting CO₂ into geological structures (such as deep saltwater layers, abandoned oil and gas reservoirs, and unexplainable coal seams) combined with cap rock traps. There are four main mechanisms of CO₂ storage in the formation: structural storage, residual storage, dissolution storage, and mineral storage. After CO₂ injection, it is prevented from being transported upward mainly by high capillary forces of the cap, partially dissolved in water by the solubility of CO₂ in salt water, disconnected by capillary forces of the pore structure and retained in the pores, and stored in the formation by chemical reactions to generate new substances [5, 6]. Capillary forces are positively correlated with interfacial tension, which is the phase behavior of the fluid and may greatly affect the effectiveness of structural and residual storage. Salt water layer CO₂ storage is a method of injecting CO₂ into deep salt water layers and permanently storing it through the above mechanisms. It is also currently the most promising CO₂ storage method [7, 8]. The study of the migration law of CO₂ and salty water two-phase fluids in the pore space is important for understanding the effect of structural and residual storage.

At present, research on CO₂ storage in salt water mainly relies on physical experimental methods and numerical simulation methods [9–11]. The research direction includes macroscopic mechanism description, storage capacity calculation, cap rock breakthrough pressure calculation, CO₂ migration law, and other aspects. There is relatively little research on the migration law and mechanism at the pore scale. Sun et al. [12] established models of different river lithofacies combinations based on numerical simulation methods to study the impact of heterogeneous river structures on CO₂ storage. The study noted that low permeability phases can hinder the vertical migration of CO₂ plumes. Baban et al. [13] used in situ NMR T1-T2 2D images to visualize fluid configuration in pore networks. The study found that in CO₂ wet samples, CO₂ is mainly residual in mesopores and micropores, while in water wet rocks, CO₂ is mainly residual

in macropores. Ren et al. [14] studied the migration law of CO₂ injection into a heterogeneous model through numerical simulation, and the study showed that the migration of CO₂ in a heterogeneous deep aquifer exhibits a significant fingering phenomenon. Afanasyev et al. [15] studied the injection of supercritical CO₂ into an inclined aquifer and proposed a simple relation to estimate the maximum gas migration distance in the upward dip direction. The above research indicates that CO₂ will migrate in the upward direction after being injected into the salt water layer, and due to its low viscosity, there is a fingering phenomenon, which is influenced by reservoir heterogeneity. The injection process is mainly influenced by residual gas burial and dissolution mechanisms. However, the aforementioned studies have all conducted simulation studies at the macro scale, and there is a lack of research on the CO₂ migration patterns in saltwater layers at the pore scale. At the macroscopic scale, the migration process of CO₂ can only reflect the flow direction of the CO₂ front, and cannot characterize the migration and capture mechanism of CO₂ in pores.

To address the above research questions, this paper establishes a numerical model for CO₂ migration. Based on a two-dimensional model of porous media, a pressure-driven approach is used to simulate the microscopic migration characteristics of CO₂ during the storage process of salt water layers at the pore scale. The CO₂ migration law is explained, and the influence of pressure and wettability on the migration law is analyzed. This study is a guide to further understanding the migration law of CO₂ in the pore space at the mine site and understanding the mechanism of structural storage and residual gas storage.

2 Numerical Simulation Methods

2.1 Numerical Model Establishment

CO₂ forms a two-phase interface with saltwater after entering the pore space, and it is transported upward under the effect of gravitational divergence. To simulate the microscopic seepage law of CO₂ in saltwater, the following assumptions need to be made:

- (1) Considering only the migration law of CO₂ in pores, without considering the chemical reactions between CO₂, water, and rock, the rock does not undergo deformation during fluid seepage;
- (2) CO₂ and salt water are assumed to be Newtonian fluid and incompressible fluid;
- (3) It is assumed that the values of interfacial tension and contact angle do not change during the two-phase displacement.

The continuity equation is used to control the mass balance of an incompressible fluid, as follows [16]:

$$\rho \nabla \cdot \mathbf{u} = 0 \quad (1)$$

where ρ is the fluid density, kgm⁻³; \mathbf{u} is the fluid velocity, ms⁻¹.

The Navier–Stokes equation is used to control the momentum balance of the two-phase fluid, as follows:

$$\rho \frac{\partial \mathbf{u}}{\partial t} + \rho(\mathbf{u} \cdot \nabla)\mathbf{u} = \nabla \cdot \left\{ -p\mathbf{I} + \mu \left[\nabla \mathbf{u} + (\nabla \mathbf{u})^T \right] \right\} + \mathbf{F}_{st} + \rho \mathbf{g} \quad (2)$$

where t equals the time, s; p is the pressure, Pa; \mathbf{I} represents the identity matrix; μ denotes the fluid viscosity, Pas; \mathbf{F}_{st} represents the surface tension acting at the interface between CO_2 and salt water, Pam^{-1} ; and \mathbf{g} is the gravity vector, ms^{-2} .

The level set method is used to describe the fluid interface and fluid convection. The interface between CO_2 and saltwater is determined by tracing the contour of the level set function $\phi = 0.5$. ϕ is 0 in salt water and 1 in CO_2 . In the transition layer near the interface, the ϕ value transitions smoothly from 0 to 1. The interface moves at fluid velocity \mathbf{u} . The equations controlling the transfer and reinitialization of ϕ are as follows [17]:

$$\frac{\partial \phi}{\partial t} + \mathbf{u} \cdot \nabla \phi - \gamma \nabla \cdot \left[\varepsilon \nabla \phi - \phi(1 - \phi) \frac{\nabla \phi}{|\nabla \phi|} \right] = 0 \quad (3)$$

where ϕ is the level set function, dimensionless; γ is the reinitialization parameter, ms^{-1} ; and ε is the interface thickness control parameter, m.

The global density and dynamic viscosity are determined by the following equations:

$$\rho = \rho_w + (\rho_{\text{CO}_2} - \rho_w)\phi \quad (4)$$

$$\mu = \mu_w + (\mu_{\text{CO}_2} - \mu_w)\phi \quad (5)$$

where ρ_w is the salt-water density, kgm^{-3} ; ρ_{CO_2} is the CO_2 density, kgm^{-3} ; μ_w is the salt-water viscosity, Pas; and μ_{CO_2} is the CO_2 viscosity, Pas.

Based on the level set function, the surface tension is calculated by the following equation:

$$\mathbf{F}_{st} = \sigma \delta k \mathbf{n} \quad (6)$$

$$\delta = 6|\phi(1 - \phi)|\nabla \phi| \quad (7)$$

$$\kappa = -\nabla \cdot \mathbf{n} \quad (8)$$

$$\mathbf{n} = \frac{\nabla \phi}{|\nabla \phi|} \quad (9)$$

where σ is the surface tension coefficient, Nm^{-1} ; δ is the Dirac δ function, dimensionless, with a nonzero value only at the fluid interface; and κ is the curvature, dimensionless.

The controlling equation for the wetted wall conditions is as follows:

$$\mathbf{u} \cdot \mathbf{n} = 0 \quad (10)$$

2.2 Two-Dimensional Model Establishment

The porous media model size is 9353 nm × 8550 nm, the conventional media diameter is 800 nm, and 11 media are randomly selected to expand the diameter by 10% and marked in purple.

The spacing between the conventional medium is 100 nm, and the spacing between the conventional medium and the expanded medium is 60 nm. The lower left side of the model is the inlet, and the lower right side is the outlet, as shown in Fig. 1.

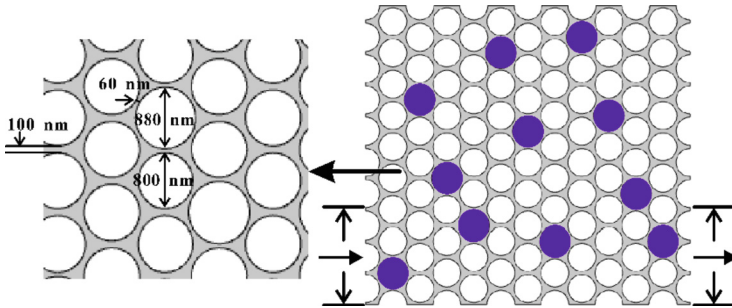


Fig. 1. Two-dimensional model diagram of porous media.

2.3 Material Parameters

The simulated environment temperature is 323.15 K, pressure is 19 MPa, salt water density is 1094.45 kgm⁻³, and viscosity is 0.7047 mPas. The density and viscosity parameters of CO₂ at different pressure conditions are shown in Table 1.

Table 1. CO₂ physical parameters under different pressure conditions.

Pressure/MPa	Density/(Kgm ⁻³)	Viscosity/(mPas)
19.8	781.83	0.06904
20	784.29	0.06948
20.3	787.90	0.07006
20.5	790.25	0.07046

2.4 Calculation Parameter Setting

The reference pressure level p_{ref} in the laminar physical field is 1.9×10^7 Pa, and the reference temperature T_{ref} and the model input temperature T are 323.15 K. The inlet relative pressure p_0 is 1×10^6 Pa, and the outlet relative pressure p_0 is 0 Pa.

Reinitialize parameters in the level set physical field γ 1 ms^{-1} , interface thickness control parameter ε set to the default value $ls_ep_default$.

In the level set physical field, the reinitialization parameter γ is 1 ms^{-1} , and the interface thickness control parameter ε is the default value $ls_ep_default$. In the initial value, the level set variable within the pore domain of the model is specified as fluid 1 (salt water), and the injected phase at the inlet is fluid 2 (CO_2).

The boundary condition of the wetting wall is the default Navier slip, and the gas phase contact angle is 120° . The surface tension coefficient of the two phases is 35 mNm^{-1} .

2.5 Grid Division Parameters

The mesh type is triangle, the number of mesh vertices is 3711, the number of triangles is 5154, the number of edge cells is 2464, the number of vertex cells is 489, the number of cells is 5154, the average cell mass is 0.7573, and the mesh area is $2.256 \times 10^7 \text{ nm}^2$.

3 Results and Discussion

3.1 Microscopic Migration Law of CO_2 Storage in the Salt Water Layer

Storage of CO_2 in the saltwater layer includes the process of displacement and suction. The displacement process is the first stage, in which CO_2 displaces salt water. The inhalation process is the second stage, in which the salt water displaces the CO_2 . The displacement process ends when the gas drive water reaches 98% gas content at the outlet. The suction process continues the displacement process, and the water drive gas ends when the water cut at the outlet reaches 98%. The gas saturation of the model at the end of the displacement process is defined as the maximum burial rate, and the gas saturation of the model at the end of the suction process is defined as the residual gas burial rate.

Figure 2 shows the two-phase migration diagram of the displacement process after CO_2 injection. Pure red represents salt water, while pure blue represents CO_2 . When the color is between red and blue, it is the interface where the two phases transition, and the color code is the volume fraction of salt water. The figure shows that when CO_2 is

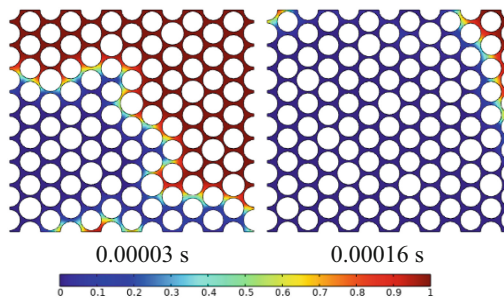


Fig. 2. Two-phase migration diagram of the displacement process (unit: dimensionless).

injected and pushed toward the right outlet, it will simultaneously migrate toward the top of the model under the effect of the two-phase density difference. After CO₂ breaks through the mainstream line at the bottom, it will displace salt water diagonally upward, and the displacement will end at 0.00016 s. The residual water is mainly distributed in the blind end area in the upper left corner and the unaffected area in the upper right corner.

Figure 3 shows the two-phase migration diagram during the suction process of salt water, with the same color representation as Fig. 2. As seen from the figure, the salt water suction approximates a fan shape advancing forward and will displace the CO₂ when it reaches the outlet and will combine with the boundary to close part of the CO₂ when it reaches the top of the model. When the salt water converges with the residual water in the upper right corner of the model, it truncates the continuous gas phase and displaces the lower gas toward the outlet under the action of gravity and capillary force, and the upper gas eventually accumulates mostly in the upper right corner of the model under hydraulic and porous media trapping. The suction process ended at 0.00027 s.

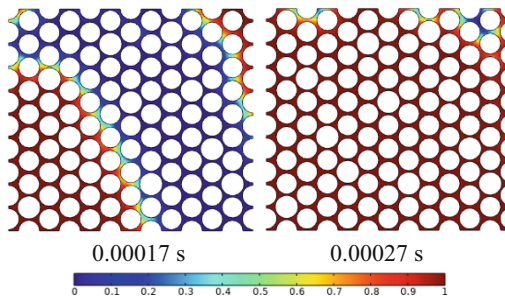


Fig. 3. Two-phase migration diagram of the suction process (unit: dimensionless).

3.2 Effect of Different Factors on Microscopic Migration Law

Effect of Injection Pressure on Microscopic Migration Law. To study the effect of injection pressure on microscopic migration laws, injection pressures of 19.8, 20, 20.3, and 20.5 MPa are selected to study the seepage characteristics of the displacement and suction processes.

Figure 4 shows the gas saturation diagram of the entire process under different injection pressure conditions. The figure shows that the gas saturation in the first stage of the displacement process first rapidly increases, and then the increase amplitude slows down. After the second stage of the suction process begins, the gas saturation first rapidly decreases and then gradually flattens out in the region. An increase in injection pressure will reduce the entire displacement time and increase the residual gas burial rate. At injection pressures of 19.8, 20, 20.3, and 20.5 MPa, the maximum burial rates are 77.84%, 93.42%, 87.85%, and 89.77%, respectively, and the residual gas burial rates are 7.88%, 3.04%, 4.24%, and 4.29%, respectively. As the injection pressure increases, the

maximum burial of CO_2 at the end of displacement first increases, then decreases, and then increases in a fluctuating manner. When the pressure is low, increasing the pressure will increase the swept area of CO_2 ; When the pressure is high, increasing the pressure will cause the formation of the mainstream channel earlier, exacerbate gas channeling, and reduce the affected area. As the injection pressure increases, the residual gas burial rate first decreases and then increases. When the suction pressure is low, increasing the pressure will increase the injection time and reduce the residual gas burial rate; When the pressure is high, increasing the pressure will shorten the time of the suction process, reduce the gas discharge volume, and increase the residual gas volume.

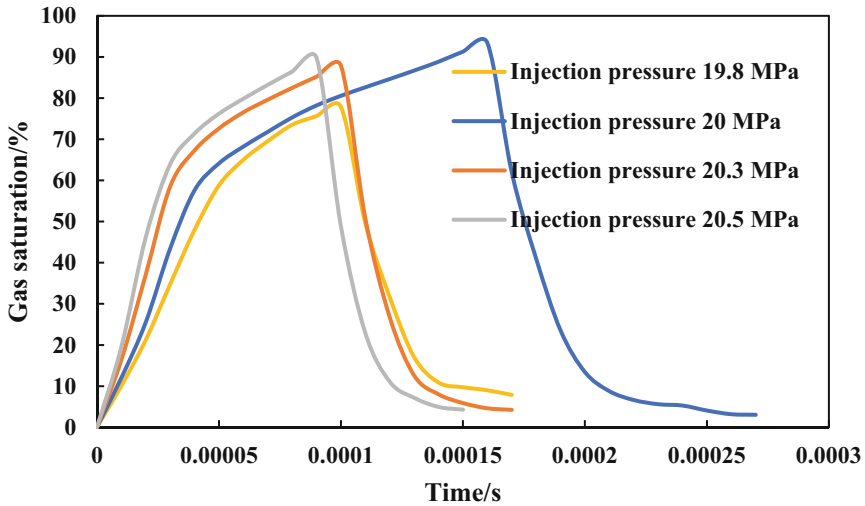


Fig. 4. Gas saturation diagram of the entire process under different injection pressure conditions.

Effect of Wettability on Microscopic Migration Law. To study the effect of wettability on microscopic migration laws, water phase contact angles of 45° , 60° , 75° , and 90° are selected to study the seepage characteristics of displacement and suction processes.

Figure 5 shows the gas saturation diagram of the entire process under different water phase contact angles. It can be seen from the figure that as the water phase contact angle increases, the displacement process time decreases and the suction process time increases. An increase in the contact angle of the water phase will gradually reduce the maximum burial rate, and the residual gas burial will first increase and then decrease. The maximum burial rates are 91.51%, 87.85%, 85.3%, and 85.2% at water phase contact angles of 45° , 60° , 75° , and 90° , respectively, and the residual gas burial rates are 3.15%, 4.24%, 4.31%, and 4.15%, respectively. An increase in the contact angle of the water phase will reduce the hydrophilicity of the wall, making it easier for CO_2 to flow out to the outlet during the displacement process, gradually reducing the maximum burial rate. An increase in the contact angle of the water phase will reduce the capillary force, and the residual gas burial rate will increase at 45° . The increase in the water phase contact

angle increases the suction process time, more gas is expelled, and the residual gas burial rate tends to decrease at 90° .

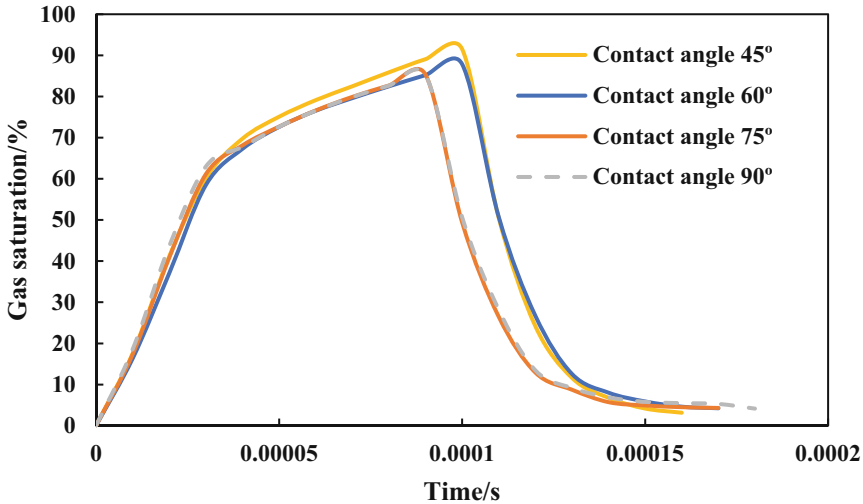


Fig. 5. Gas saturation diagram of the entire process under different water phase contact angles.

4 Conclusion

The following conclusions are obtained from the simulation of the displacement process and the suction process of CO_2 storage in salt water:

- (1) During the displacement process, when CO_2 is injected and pushed toward the right outlet, it will simultaneously migrate toward the top of the model under the effect of the two-phase density difference. The residual water is mainly distributed in the blind end area in the upper left corner and the unaffected area in the upper right corner.
- (2) During the suction process, the salty water is sucked in and pushed forward in an approximate fan shape, and when it reaches the top of the model, it will cut off the continuous phase of CO_2 with the residual water and combine with the boundary to trap part of the CO_2 so that the CO_2 is trapped at the edge and angle.
- (3) The increase in injection pressure will reduce the full process displacement time and increase the residual gas burial rate. The residual gas burial rate decreases and then increases with increasing injection pressure.
- (4) When the contact angle of the water phase increases, the displacement process time is shortened, and the suction process time is increased. An increase in the contact angle of the water phase will gradually reduce the maximum burial rate, and the residual gas burial will first increase and then decrease.

Acknowledgments. The project is supported by National Natural Science Foundation (Number 51974343).

References

1. Zhang, K., Lau, H., Chen, Z.: CO₂ enhanced gas recovery and sequestration as CO₂ hydrate in shallow gas fields in Alberta, Canada. *J. Nat. Gas Sci. Eng.* **103**, 104654 (2022)
2. Cui, Y., Bai, J., Liao, S., et al.: Suggestions on the development of environmental monitoring technology of CO₂ geological storage and leakage under the background of China's "Double-Carbon" strategy. *Atmosphere* **14**(1), 51 (2022)
3. Chen, Z., Zhou, Y., Li, H.: A review of phase behavior mechanisms of CO₂ EOR and storage in subsurface formations. *Ind. Eng. Chem. Res.* **61**(29), 10298–10318 (2022)
4. Zhang, K., Lau, H.: Regional opportunities for CO₂ capture and storage in Southeast Asia. *Int. J. Greenhouse Gas Control* **116**, 103628 (2022)
5. Chenrai, P., et al.: A preliminary assessment of geological CO₂ storage in the Khorat Plateau, Thailand. *Front. Energy Res.* **10**, 1164 (2022)
6. Ren, D., Wang, X., Kou, Z., et al.: Feasibility evaluation of CO₂ EOR and storage in tight oil reservoirs: a demonstration project in the ordos basin. *Fuel* **331**, 125652 (2023)
7. Peter, A., Yang, D., Eshiet, K., et al.: A review of the studies on CO₂–brine–rock interaction in geological storage process. *Geosciences* **12**(4), 168 (2022)
8. Jung, S.: Expansion of geological CO₂ storage capacity in a closed aquifer by simultaneous brine production with CO₂ injection. *Sustainability* **15**(4), 3499 (2023)
9. Wang, G., et al.: Integrated numerical simulation of CO₂ flooding - heat recovery and storage in high temperature reservoir. *Pet. Sci. Technol.* **41**(12), 1250–1271 (2022)
10. Qi, S., et al.: Experimental investigation on the CO₂ effective distance and CO₂-EOR storage for tight oil reservoir. *Energy Fuels* **37**(1), 339–349 (2022)
11. Li, Z., et al.: Investigation of CO₂ storage and EOR of alternating N₂ and CO₂ injection using experiments and numerical simulation. *Fuel* **340**, 127517 (2023)
12. Sun, X., et al.: Effects of fluvial sedimentary heterogeneity on CO₂ geological storage: Integrating storage capacity, injectivity, distribution and CO₂ phases. *J. Hydrol.* **617**, 128936 (2023)
13. Baban, A., et al.: Effect of organic acids on CO₂ trapping in carbonate geological formations: pore-scale observations using NMR. *Energy Fuels* **37**(4), 2983–2992 (2023)
14. Ren, J., et al.: Characterization method and application of heterogeneous reservoir based on different data quantity. *Lithosphere* **2022**, 8267559 (2022)
15. Afanasyev, A., Vedeneva, E., Grechko, S.: Scaling analysis for a 3-D CO₂ plume in a sloping aquifer at a late stage of injection. *J. Nat. Gas Sci. Eng.* **106**, 104740 (2022)
16. Eiswirth, R., et al.: Experimental and numerical investigation of a free rising droplet. *Chem. Eng. Process.-Process Intensificat.* **50**(7), 718–727 (2011)
17. Hysing, S.: Mixed element FEM level set method for numerical simulation of immiscible fluids. *J. Comput. Phys.* **231**(6), 2449–2465 (2012)